Climate Dynamics
https://doi.org/10.1007/s00382-024-07343-7

ORIGINAL ARTICLE

Triggering effects of spring thermal contrast between Yun-Gui Plateau and Beibu Gulf on the interannual variations of South China Sea summer monsoon onset dates

Zizhen Dong[1,2] · **Jie Cao**[1,2] · **Shu Gui**[1,2] · **Ruowen Yang**[1,2]

Received: 27 March 2024 / Accepted: 14 July 2024

Abstract
Based on observation analysis and numerical simulation, this study reveals that the spring land-sea thermal contrast between Yun-Gui Plateau and Beibu Gulf has a significant triggering impact on the variations of South China Sea summer monsoon onset dates (SCSSMOD) at the interannual timescale. The March–April thermal contrast with warm Yun-Gui Plateau and cold Beibu Gulf results in an anomalous low-level anticyclone over the western North Pacific, which in turn causes the active convection in the tropical western Pacific via the friction convergence. This active convection persists into May and moves northward towards the South China Sea. It subsequently excites an anomalous low-level cyclone in situ via the Matsuno-Gill mechanism. Then, the western Pacific subtropical high is tending to retreat eastward and the westerly wind anomalies occupy the South China Sea, promoting an early SCSSMOD. When the thermal contrast reverses, the SCSSMOD is inclined to be late. The effects mentioned above are independent of ENSO, indicating an effective indicator for monitoring and predicting the SCSSMOD at the interannual timescale.

Keywords Yun-Gui Plateau · Beibu Gulf · South China Sea summer monsoon · Onset dates · Thermal contrast · Interannual

1 Introduction

The South China Sea summer monsoon (SCSSM) is a crucial component of the East Asian summer monsoon (Xie et al. 1998; Wang et al. 2009; He et al. 2017). Its onset signifies the adjustment of large-scale circulation from winter to summer season and denotes the arrival of rainy season in East Asia (Lau and Yang 1997; Ding and Chan 2005; Ding et al. 2015; Hu and Chen 2018). After the SCSSM onset, the monsoon circulations in East Asia shift northward, the western Pacific subtropical high retreats eastward (He et al. 2006; Liu et al. 2016; Choudhury et al. 2022), and the Meiyu belt establishes (Wang and LinHo 2002; Chen et al. 2012; Shao et al. 2014; Jiang et al. 2018; Feng et al. 2021). Hence, it is important and necessary to understand the processes that drive the SCSSM onset.

Statistically, the average SCSSM onset date (SCSSMOD) emerges at pentad 28 (May 16–20) (Wang et al. 2004; Liu et al. 2015; Xu and Li 2021; Chen and Wang 2023). A large number of studies have indicated that the thermodynamic factors associated with the tropical Indian Ocean, tropical Pacific, and Tibetan Plateau are important to impact the SCSSMOD variations at the interannual timescale (Yuan et al. 2008; Shao et al. 2015; Luo et al. 2016; Hu and Chen 2018; Huangfu et al. 2018; Liu and Zhu 2019; Feng et al. 2021; Chen et al. 2022; Xu et al. 2022), and the latter then cause significant East Asian climate anomalies. For example, a delayed SCSSMOD can result in increased rainfalls surrounding the Yangtze River (He and Zhu 2015; Jiang et al. 2018), while an early SCSSMOD may cause decreased summer rainfalls over the subtropical regions (Hung et al. 2006). Among various factors, El Niño – Southern Oscillation (ENSO) is of particular importance to drive the SCSSMOD variations at the interannual timescale. An early SCSSMOD follows a preceding La Niña winter and a late SCSSMOD

✉ Jie Cao
caoj@ynu.edu.cn

1 Yunnan Key Laboratory of Meteorological Disasters and Climate Resources in the Greater Mekong Subregion, Yunnan University, Kunming, China

2 Department of Atmospheric Sciences, Yunnan University, Kunming, China

Published online: 25 July 2024

follows a preceding El Niño winter (Zhou and Chan 2007; Hu and Chen 2018; Hu et al. 2020, 2022). There are two ways that ENSO can affect the SCSSMOD. On the one hand, the El Niño can modulate the Pacific Walker cell and cause the suppressive convections and downward motions over the Indo-Pacific warm pool (Webster and Yang 1992). On the other hand, the El Niño's cold sea surface temperature (SST) over the tropical western Pacific can cause the low-level Rossby anticyclonic circulation on the northwest side (Hu et al. 2022). Both effects lead to enhanced easterly and decreased precipitation anomalies over the South China Sea (SCS), resulting in a delayed SCSSMOD (Luo et al. 2016).

Nevertheless, the relationship between the SCSSMOD and ENSO is unstable and is experiencing a weakening phase in recent years (Hu et al. 2020; Jiang and Zhu 2021; Chen et al. 2022). For example, following the La Niña winter in 2017/2018, the SCSSMOD was exceptionally delayed (Lu et al. 2020). Following the 2018/2019 El Niño winter, the SCSSMOD was unusually early (Hu et al. 2020). Previous studies have attributed such a disconnected relationship to the mid-high latitude circulation systems, the monsoon onset vortex, and the intraseasonal oscillation (Liu and Zhu 2019; Deng et al. 2020; Hu et al. 2020). Given that ENSO is typically considered as the primary seasonal predictor for the SCSSMOD at the interannual timescale (Zhu and Li 2017; Martin et al. 2019), their diminishing relation indicates that it may be challenging to perform a skilful seasonal prediction for SCSSMOD if solely focusing on ENSO. Hence, the alternative predictors instead of ENSO should be explored.

As the East Asian summer monsoon is primarily considered as the atmospheric response to land-sea thermal contrast (Wu et al. 2012), the potential indicators can be found from the atmospheric thermal conditions. Previous studies indicated that a significant surface temperature gradient between the Indochina Peninsula and the adjacent SCS emerges before the SCSSM onset (Chow et al. 2006; Wang et al. 2017; Li et al. 2020; Chen and Wang 2023). When the Indochina Peninsula warms faster and earlier than SCS, the SCSSMOD tends to be earlier (Liu et al. 2009). These studies suggest that the land-sea thermal condition is crucial to impact the SCSSMOD. Despite these innovative works, there is still insufficient understating of the precursor thermal signals associated with the variations of SCSSMOD at the interannual timescale. This lack of understanding hinders the monitoring and prediction efforts related to SCSSMOD.

The Yun-Gui Plateau (YunGuiP: 22°–27°N, 105°–110°E, Fig. 1), including most of territories of Yunnan and Guizhou Provinces in Southwest China, is a region described as a broad transitional zone separating the western North Pacific (WNP) summer monsoon from the Indian summer monsoon (Wang and LinHo 2002). The YunGuiP is also a primary part of the low-latitude plateau of Southeast Asia, a warmer and wetter highland region (Yang et al. 2023, 2024). In

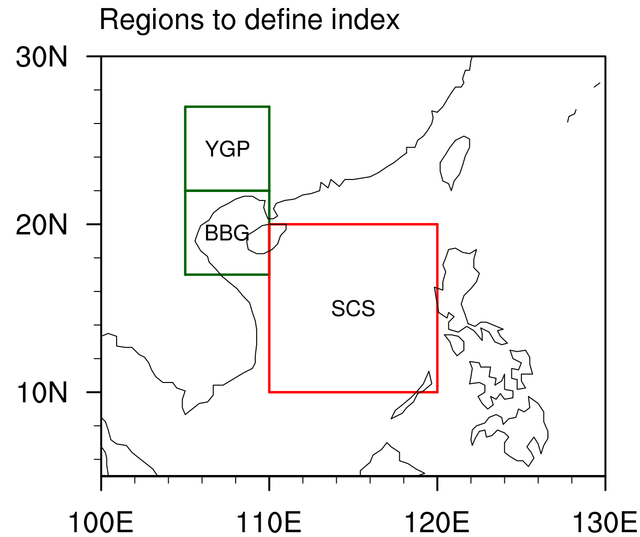

Fig. 1 Regions to define the YunGuiP (upper green: 22°–27°N, 105°–110°E) and BeibuG (lower green: 17°–22°N, 105°–110°E) thermal indices. The red rectangle represents the monitoring region over the SCS (10°–20°N, 110°–120°E)

spring, the YunGuiP and the low-latitude plateau of Southeast Asia act as a heat source (Fig. 2a), resulting in the significant release of atmospheric diabatic heating, which then affects the East Asian summer circulations (Yang et al. 2024), the Meiyu onset (Wen et al. 2024a), and the summer East Asian–Pacific teleconnection (Wen et al. 2024b). Due to the specific thermal condition and climate effect in YunGuiP, its thermal contrast with the adjacent seas such as the Beibu Gulf (BeibuG: 17°–22°N, 105°–110°E, Fig. 1) may affect the interannual variations of downstream circulation system, i.e., the SCSSM, to a certain extent. Since the purpose of the study is to propose an effective indicator for the SCSSMOD based on the understanding of land-sea thermal contrast, two scientific issues should be addressed here: (1) Whether the thermal contrast between the YunGuiP and BeibuG can significantly affect the SCSSMOD variations at the interannual timescale? (2) If so, what are the potential triggering mechanisms? This study aims to answer these questions.

2 Data and methodology

2.1 Data and methods

The study uses the monthly outputs of the Global Precipitation Climatology Project (GPCP, Adler et al. 2003) Combined Precipitation Dataset and the NOAA outgoing longwave radiation dataset (OLR, Liebmann and Smith 1996), both of which are spatially gridded into $2.5° \times 2.5°$ from 1979 to the present. The atmospheric circulation data

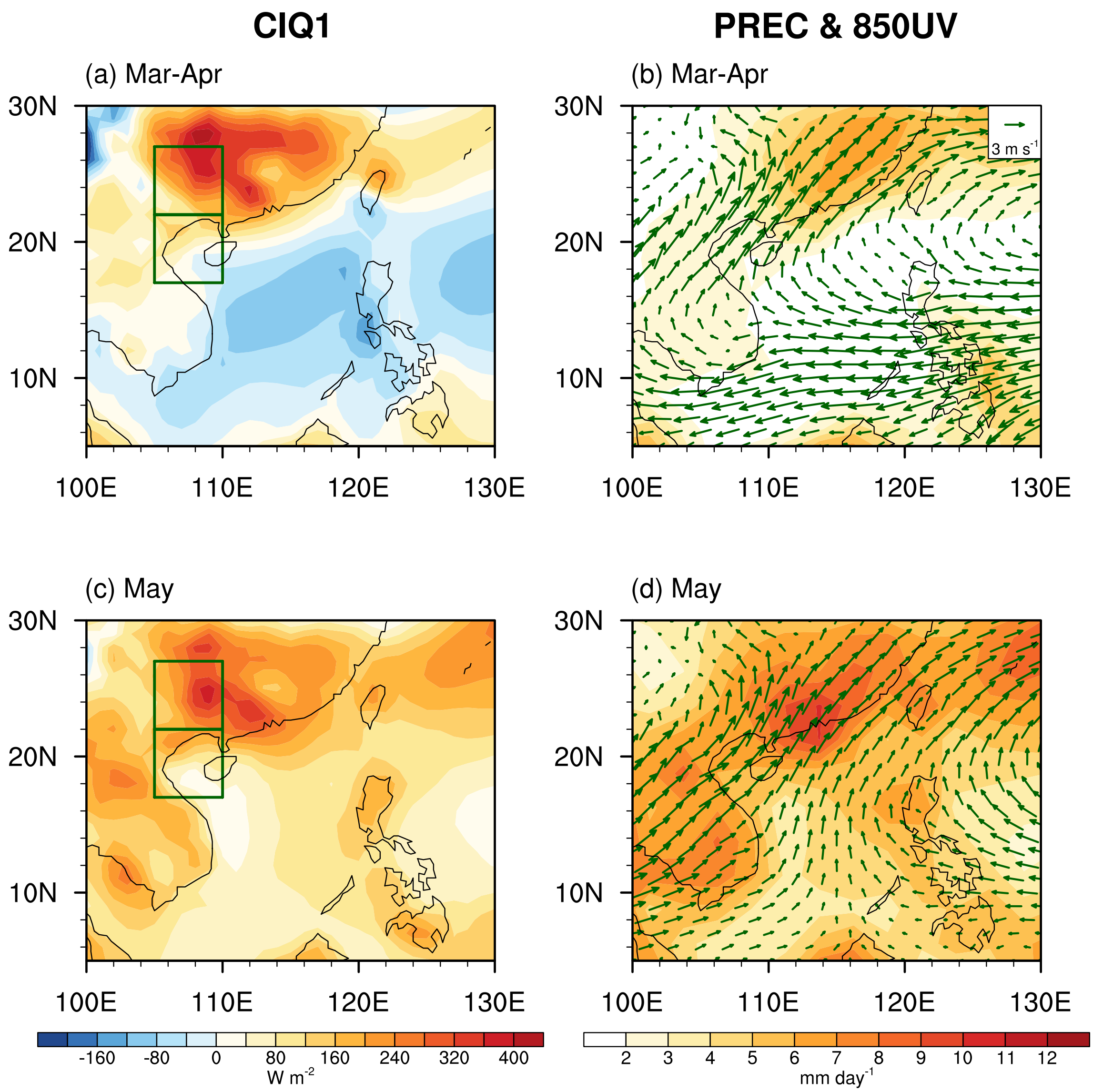

Fig. 2 Climatological distribution of **a** CIQ1 [shading, shade interval (SI) = 40 W m^{-2}], and **b** 850 hPa winds (vector, unit: 3 m s^{-1}) and precipitation (shading, SI = 1 mm day^{-1}) in March–April during 1979–2019. **c**–**d** are the same as (**a**–**b**), but in May. The upper and lower green rectangles in (**a** and **c**) represent the regions of YunGuiP and BeibuG, respectively

is derived from the fifth version of the ECMWF reanalysis dataset (ERA5, Hersbach et al. 2020). The ERA5 dataset is gridded at 1.0° × 1.0° and covers the period from 1979 to 2019. In the study, the period 1979–2019 is focused on.

Following the criterion of National Climate Centre in China, the SCSSMOD is defined as the first pentad when 850 hPa zonal winds area-mean over the SCS (10°–20°N, 110°–120°E, Fig. 1) convert from easterly to westerly winds. Additionally, the 850 hPa potential pseudo-equivalent temperature exceeds 340 K. These features must persist at least three consecutive pentads (Jiang et al. 2018). The atmospheric apparent heat source of the thermodynamic equation, *Q1*, is calculated using the 6-h ERA5 data following the method of Yanai et al. (1992):

$$Q_1 = C_p\left(\frac{p}{p_0}\right)^k\left(\frac{\partial\theta}{\partial t} + \vec{V}\cdot\nabla\theta + \omega\frac{\partial\theta}{\partial p}\right) \tag{1}$$

where C_p is the specific heat capacity at constant pressure, $k = R/C_p$, R is the gas content, p is the pressure, and p_0 is the 1000 hPa pressure. θ is the potential temperature, $\vec{V}$ is the horizontal winds, ∇ is the gradient, and ω is the vertical pressure velocity. The terms in parentheses represent the local changes of potential temperature, the advection effects and vertical transport of potential temperature, respectively.

Then, the atmospheric thermal conditions in YunGuiP and BeibuG are represented by the column-integrated Q1 from Earth's surface to 125 hPa (CIQ1, Gui et al. 2022; Wen et al. 2024b), which can be expressed as follows:

$$< Q_1 >= \frac{1}{g}\int_{p_t}^{p_s} Q_1 d_p \quad (2)$$

As the SCSSMOD mostly occur in May (Yuan et al. 2008; Kajikawa and Wang 2012; Liu et al. 2015; Xu and Li 2021), we focus on the precursory thermal contrast between YunGuiP and BeibuG in preceding spring (i.e., March–April). In addition, to highlight the interannual variability and to avoid the possible influence of global warming, we remove the linear trends before conducting analysis. Correlation and regression analyses are used in the study and their significance levels are determined by the two-tailed Student's *t*-test.

2.2 Numerical model validation

The study applies the European Centre-Hamburg atmospheric model developed by the MPI-M version 6.3 (ECHAM6.3, Giorgetta et al. 2013) to validate the observed conclusions. The ECHAM6.3 model, which is widely used in climate researches (Gui et al. 2020; Ma and Jiang 2020; Dong et al. 2023), has a horizonal resolution of T63 and a vertical resolution of 47 hybrid sigma-levels. The global climatology of monthly sea ice extent and SST are set as model's boundary conditions. In the study, two sensitivity experiments are conducted, the positive phase and negative phase experiments (Posi-exp and Nega-exp hereafter). These experiments are forced by the observed spring Q1 anomalies at levels in YunGuiP and BeibuG (see Sect. 4.2 for details). Each experiment in ECHAM6.3 is continuously integrated for 20 years, and the last 10 years are used for analysis.

3 Association between the YunGuiP-BeibuG thermal contrast and the SCSSMOD at the interannual timescale

Climatologically, YunGuiP in spring is characterized by a significant heat source extending northward and eastward, and approaches the maximum heating centre in South China (Fig. 2a). In contrast, south of YunGuiP such as the BeibuG and SCS are the heat sink regions. This large-scale thermal configuration of warm land and cold sea favours the low-level clockwise circulation that prevails over the subtropical WNP (Fig. 2b). Associated with the clockwise circulation in the lower troposphere, there are strong rainfalls over the Maritime Continent that are resulted from the easterly convergence along the equator (Li et al. 2020). In May, both land and marine areas in East Asia become heat sources, with the ocean warms faster, particularly over the SCS (Fig. 2c). Such atmospheric heating distribution in May largely weakens the original land-sea thermal contrast, leading to the eastward retreat of the western Pacific subtropical high (Fig. 2d). At the same time, strong southwesterlies dominate the Indochina Peninsula, causing the strengthening of precipitation and westerly winds over the SCS and denoting the SCSSM onset in May (Fig. 2d). The increased precipitation over the SCS is primarily due to the low-level southwest warm-humid flows from the Bay of Bengal and the northward movement of precipitation from the Maritime Continent. Note that above seasonal variations of precipitation and circulations coincide well with those of atmospheric thermal conditions in East Asia from spring to May, indicating a close association between the regional land-sea thermal contrast in East Asia and the SCSSMOD.

The SCSSMOD presents clearly interannual variations during 1979–2019 (Fig. 3). The extreme early onset dates occur at 1994, 1996, 2001, 2008, 2011, and 2019 and extreme late onset dates appear at 1982, 1987, 1989, 1991, 2014, and 2018, These extreme early/late onset dates are defined when the actual dates are 1.5 pentad smaller/larger than the average date during 1979–2019 (i.e., pentad 28.5). To determine if there is a strong correlation between the YunGuiP-BeibuG thermal contrast in spring and the SCSSMOD at the interannual timescale, we define a land-sea thermal contrast index as the difference of area-mean CIQ1 anomalies between YunGuiP and BeibuG during March–April. A positive index indicates a warm land and

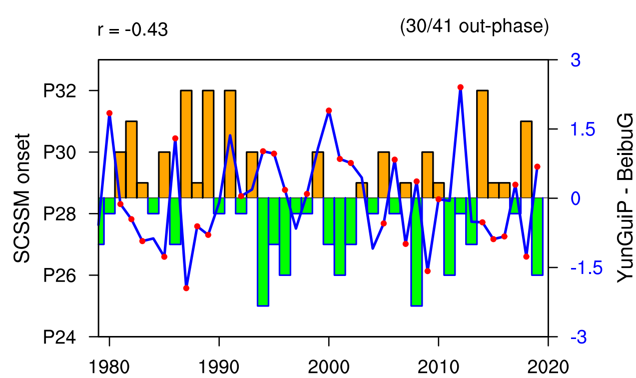

Fig. 3 Time series of the SCSSMOD (bar, left y-axis) and the normalized YunGuiP-BeibuG thermal contrast index (blue line, right y-axis) during 1979–2019, respectively. The horizontal line represents the average SCSSSM onset date with the value of pentad 28.5. The labels in left y-axis indicate the onset pentad of SCSSM. The left title denotes the correlation coefficient between two indices, and the right title indicates the number of anti-phase years (red points inside) between the early SCSSMOD and the positive thermal contrast or between the late SCSSMOD and the negative thermal contrast

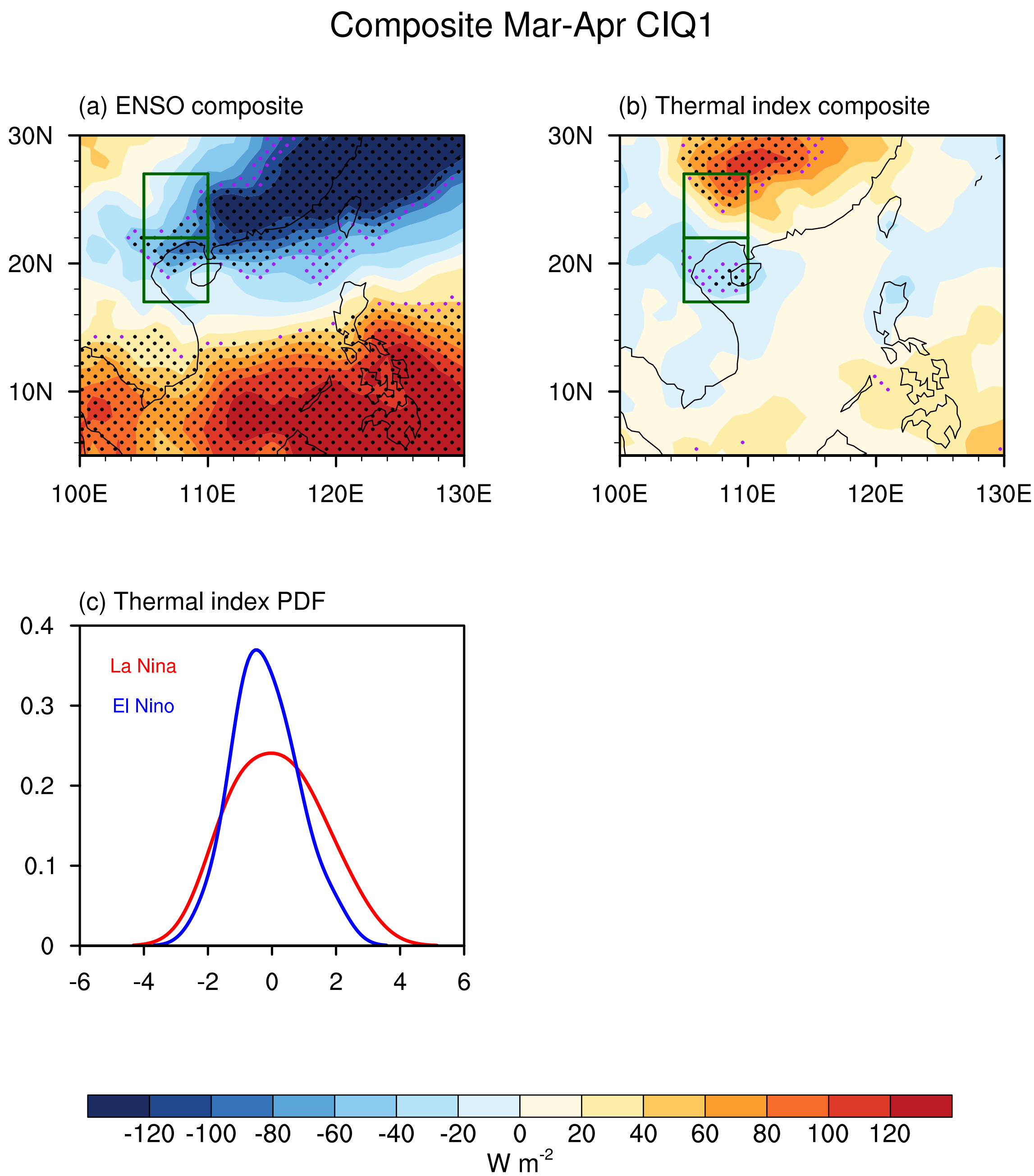

Fig. 4 Composite maps of spring CIQ1 anomalies (shading, SI = 20 W m^{-2}) **a** between the preceding La Niña and El Niño winters, and **b** between the positive and negative YunGuiP-BeibuG thermal contrast phases, respectively. The purple and black dots indicate values statistically significant at the 10% and 5% significance levels, respectively. The green rectangles indicate the regions of YunGuiP and BeibuG, respectively. **c** PDF of thermal contrast index with respect to the preceding El Niño (blue) and La Niña (red) winters

cold sea, while a negative index denotes the opposite condition. The correlation coefficient between the SCSSMOD and the YunGuiP-BeibuG thermal index is −0.43 during 1979–2019 statistically significant at the 5% significance level, explaining about 18.49% of the total variance. In addition, out of the total 41 years, there are 30 years (about 73.17%) of monsoon onset dates exhibiting the out-phase relation with the thermal contrast index. A warm thermal condition in YunGuiP and cold condition in BeibuG may correspond to an early SCSSMOD and vice versa. These results indicate that the YunGuiP-BeibuG thermal contrast qualitatively tracks well with the interannual variations of the SCSSMOD.

Early studies suggested that ENSO in preceding winter can significantly impact the SCSSMOD at the interannual timescale (Martin et al. 2019; Chen et al. 2022). According

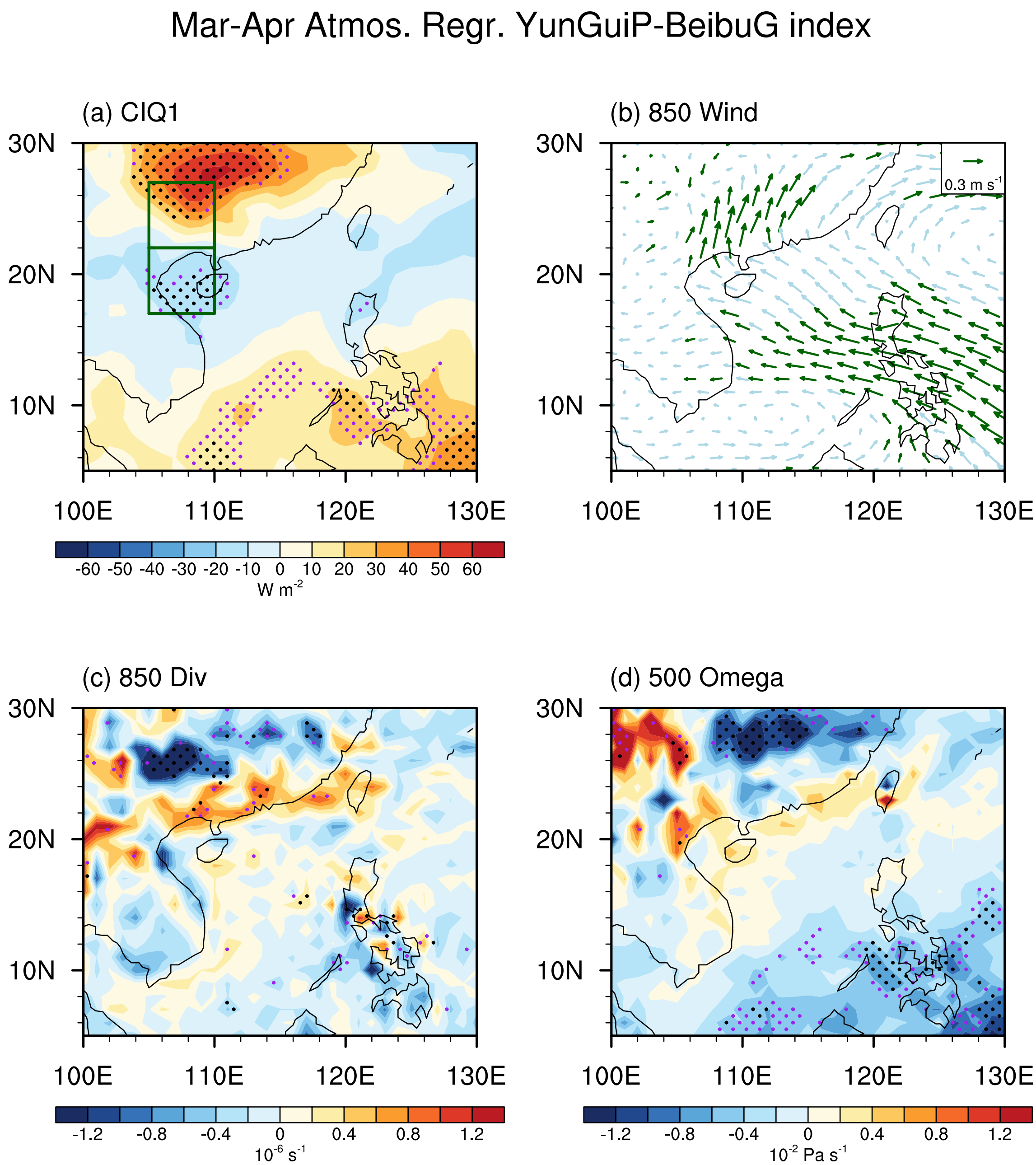

Fig. 5 Regression of the March–April **a** CIQ1 (shading, SI = 10 W m^{-2}), **b** 850 hPa winds (vector, unit: 0.3 m s^{-1}), **c** 850 hPa divergence (shading, SI = 0.2×10^{-6} s^{-1}), and **d** 500 hPa vertical velocity (shading, SI = 0.2×10^{-2} Pa s^{-1}) onto the normalized thermal contrast index during 1979–2019, respectively. The purple and black dots indicate values statistically significant at the 10% and 5% significance levels, respectively. The green rectangles in (**a**) indicate the regions of YunGuiP and BeibuG, respectively. The green and light-blue vectors in (**b**) represent values above and below the 10% significance levels, respectively

to the NOAA CPC definition, our research period from 1979 to 2019 includes 14 El Niño (1979/1980, 1982/1983, 1986/1987, 1987/1988, 1991/1992, 1994/1995, 1997/1998, 2002/2003, 2004/2005, 2006/2007, 2009/2010, 2014/2015, 2015/2016, and 2018/2019) and 13 La Niña (1983/1984, 1984/1985, 1988/1989, 1995/1996, 1998/1999, 1999/2000, 2000/2001, 2005/2006, 2007/2008, 2008/2009, 2010/2011, 2011/2012, and 2017/2018) winters. The SCSSMOD is found to be late following most El Niño winters and is early following most of La Niña winters, about 64.29% (9 out of 14) and 61.54% (8 out of 13), respectively. As the YunGuiP-BeibuG thermal contrast may also affect the SCSSMOD

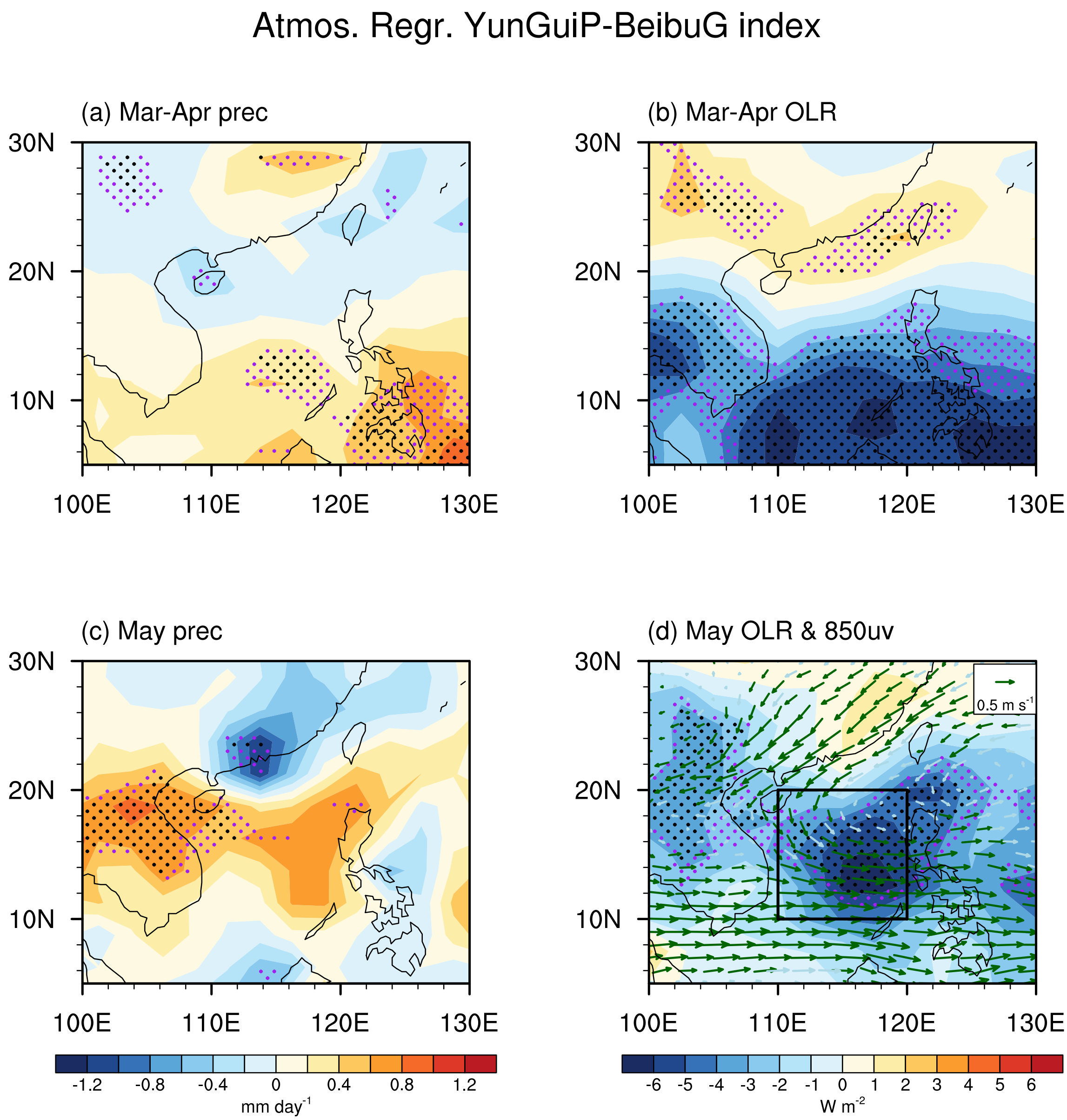

Fig. 6 Same as Fig. 5, but for the regression of **a** the March–April precipitation (shading, SI = 0.2 mm day^{-1}), **b** the March–April OLR (shading, SI = 1 W m^{-2}), **c** the May precipitation (shading, SI = 0.2 mm day^{-1}), and **d** the May OLR (shading, SI = 1 W m^{-2}) overlaid by the 850 hPa wind (vector, unit: 0.5 m s^{-1}) anomalies, respectively. The black rectangle in (**d**) denotes the monitoring region over the SCS (10°–20°N, 110°–120°E)

(Fig. 3), it is essential to explore the possible relationship between these two indicators. Figure 4 displays the composite maps of spring CIQ1 anomalies between the preceding La Niña and El Niño winters, and that between the positive and negative thermal contrast index, respectively. It can be observed that during La Niña years, the CIQ1 anomalies are higher-than-normal in the tropical western Pacific (Fig. 4a). This is due to enhanced precipitation and active convection related to the strengthening of Pacific Walker cell (Feng et al. 2010; Dong et al. 2021). These CIQ1 anomalies then lead to the reversed counterparts over the WNP due to the excited local Hadley circulation, which cause atmospheric cooling conditions in both YunGuiP and BeibuG. In contrast, during the positive phase of YunGuiP-BeibuG thermal contrast, there is an obvious difference and meridional gradient in thermal conditions between land and sea, with high-than-normal CIQ1 in YunGuiP and low-than-normal ones in BeibuG (Fig. 4b). Note that the thermal contrast

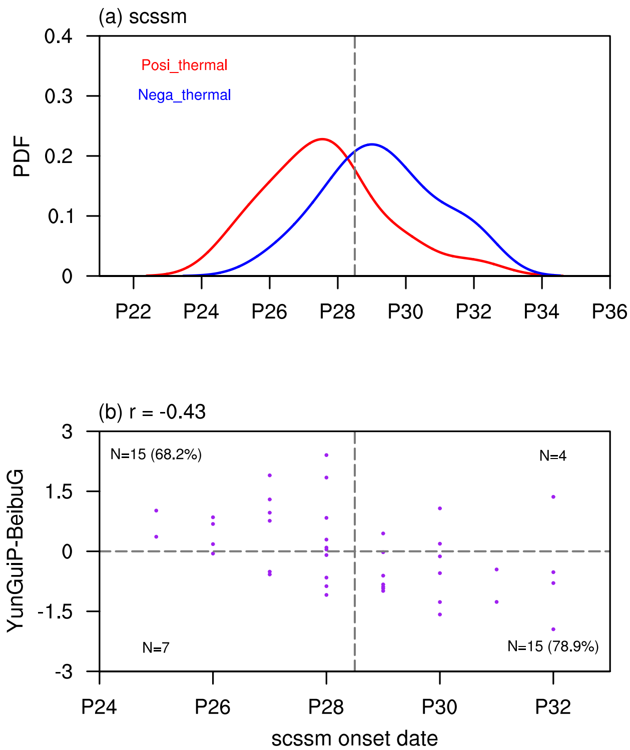

Fig. 7 **a** PDF of the SCSSMOD with respect to the positive (red line) and negative (blue line) YunGuiP-BeibuG thermal contrast. The dashed grey line denotes the average onset date with value of pentad 28.5 during 1979–2019. **b** Scatter plot of the SCSSMOD (x-axis) versus the thermal contrast index (y-axis) during 1979–2019. Horizontal and vertical dashed lines denote the zero value and the average onset date, respectively. The numbers inside denote the total years in each quadrant and the left title represents the correlation coefficient of two indices

index-associated atmospheric heating reflects stronger thermal anomalies in YunGuiP than that in BeibuG, which may due to the larger interannual standard deviation of mean CIQ1 in YunGuiP (73.8 W m^{-2}) than that in BeibuG (50.0 W m^{-2}). In total, the CIQ1 anomalies related to thermal contrast index differ significantly from those associated with ENSO, indicating that the effects of YunGuiP-BeibuG thermal contrast may not be correlated with ENSO in preceding winters. To demonstrate their uncorrelation, Fig. 4c presents the probability density function (PDF) of thermal contrast index with respect to the El Niño and La Niña winters. It is evident that the PDFs are similar and their median values are identical under different ENSO phases. Furthermore, after removing the Niño-3.4 index, the partial correlation coefficient between the SCSSMOD and the thermal contrast index remains −0.42, still statistically significant at the 5% significance level. The results imply that the potential triggering impact of YunGuiP-BeibuG thermal contrast on the SCSSMOD at the interannual timescale is independent of ENSO.

4 Triggering mechanisms of the YunGuiP-BeibuG thermal contrast on the SCSSMOD

4.1 Observation and statistical analysis

To investigate the potential triggering mechanisms of spring YunGuiP-BeibuG thermal contrast on the SCSSMOD at the interannual timescale, the regressions of spring atmospheric variables onto the normalized thermal contrast index during 1979–2019 are presented. When the thermal index is in the positive phase, both the climatological heat source in YunGuiP and the heat sink surrounding the BeibuG and SCS are significantly enhanced (Fig. 5a). This atmospheric thermal configuration largely resembles to the large-scale climatological CIQ1 distribution (Fig. 2a), thus reinforcing the mean circulation over the WNP in the lower troposphere and generating an anticyclonic anomaly there (Fig. 5b). South of the anticyclonic circulation, there are notable easterly anomalies over the tropical western Pacific, causing the convergent flows ($\partial u/\partial x < 0$) in situ (Fig. 5c) due to the friction effect (Maloney and Hartmann 1998). This in turn leads to significant ascending motions in the middle troposphere (Fig. 5d). In fact, there may be a two-way process between the large-scale anticyclonic anomaly over the WNP and the YunGuiP-BeibuG thermal contrast in spring. For example, the WNP anticyclonic anomaly can also cause the thermal heating anomalies in YunGuiP via the southwesterly winds-induced low-level convergence and ascending motion. However, only based on the statistical-observation analysis, such a two-way interaction is difficult to distinguish and separate. In the next section, we will design the numerical model experiments to confirm the observed results, especially the one-way effect associated with the forcing of YunGuiP-BeibuG thermal contrast.

Once the strong low-level convergent flows and the mid-level ascending motions emerge over the tropical western Pacific, they can lead to significantly positive precipitation anomalies and active convection there (Fig. 6a–b). The enhanced precipitation and active convection persist into May and then move northward towards the SCS (Fig. 6c–d). In May, the active convection over the SCS triggers a Matsuno-Gill response (Gill 1980; Dong et al. 2022) in the lower troposphere, resulting in a Rossby cyclonic circulation on the northwest side (Fig. 6d). This could cause the eastward retreat of western Pacific subtropical high and leads to strong and significant westerly anomalies over the SCS with the area-mean value at 0.46 m s^{-1}, thus creating a favourable environment to accelerate the seasonal transition from low-level easterly

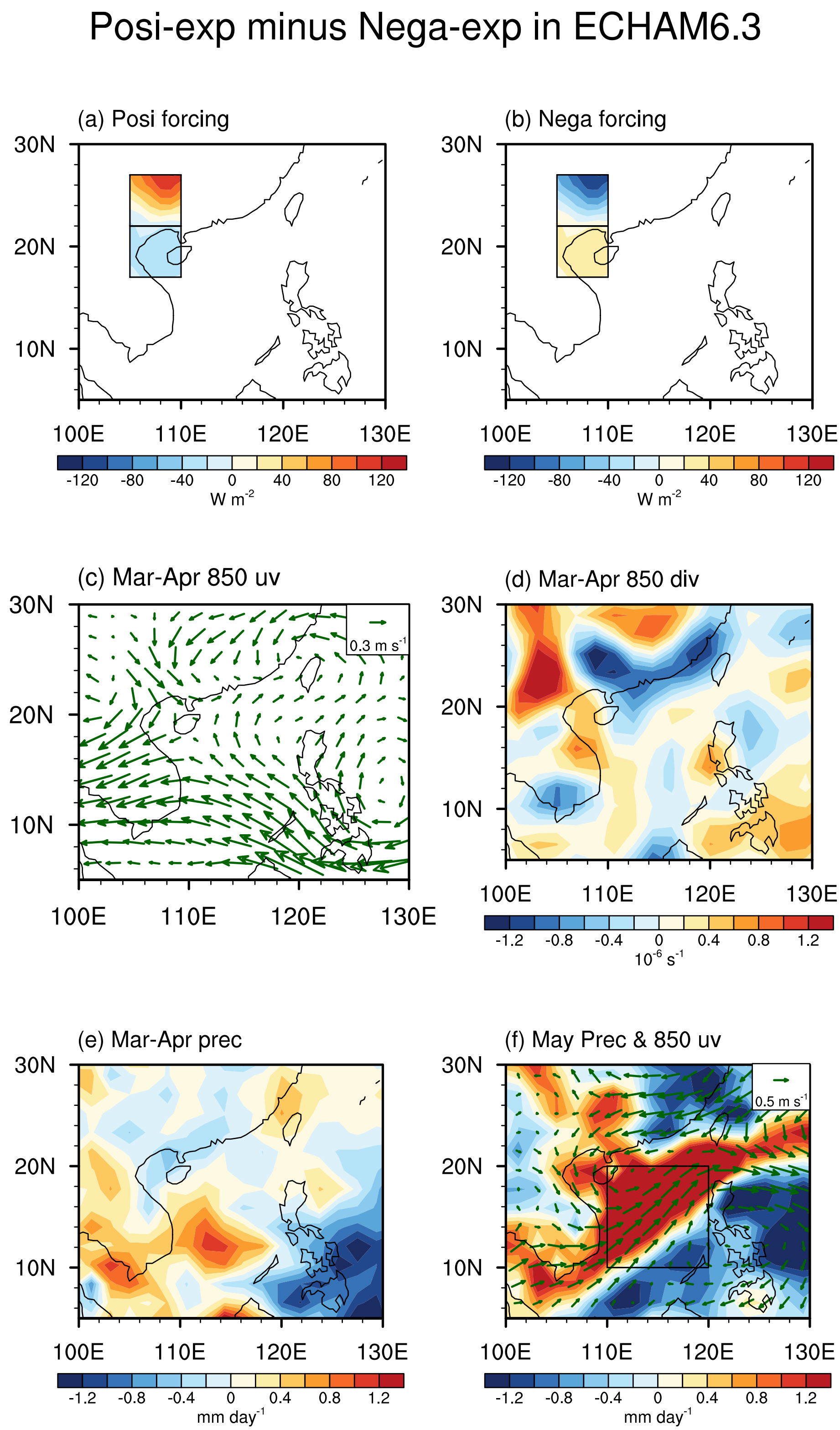

Fig. 8 The March–April forcings of CIQ1 anomalies (shading, SI = 20 W m^{-2}) in ECHAM6.3 **a** Posi-exp and **b** Nega-exp, respectively. The composite differences of **c** the 850 hPa winds in spring (vector, unit: 0.3 m s^{-1}), **d** the 850 hPa divergence in spring (shading, SI = 0.2 × 10^{-6} s^{-1}), **e** the precipitation in spring (shading, SI = 0.2 mm day^{-1}), and **f** the precipitation (shading, SI = 0.2 mm day^{-1}) superimposed by the 850 hPa winds (vector, unit: 0.5 m s^{-1}) in May between the Posi-exp and Nega-exp in ECHAM6.3, respectively. The black rectangle in (**f**) represents the SCS region

winds to westerly winds and causing an early SCSSMOD. The opposite happens when the YunGui-BeibuG thermal contrast index reverses (not shown). Hence, the spring land-sea thermal contrast between the YunGuiP and BeibuG can provide a potential indicator for SCSSMOD through aforementioned physical processes.

To examine the significance of association between the spring YunGuiP-BeibuG thermal contrast and the

Table 1 Correlation coefficients between the spring area-mean thermal contrast index in different regions and the SCSSMOD during 1979–2019

rr (thermal contrast index, SCSSMOD)						
	105-107E	105-110E	105-112E	105-115E	105-117E	105-120E
22±5N	-0.33	-0.43	-0.38	-0.37	-0.35	-0.35
22±7N	-0.22	-0.29	-0.29	-0.25	-0.23	-0.23
22±9N	-0.14	-0.22	-0.22	-0.17	-0.14	-0.14
22±11N	-0.07	-0.14	-0.12	-0.06	-0.04	-0.04
22±13N	0.01	-0.04	-0.01	0.05	0.07	0.07
22±15N	0.08	0.05	0.09	0.14	0.16	0.16

The thermal contrast index is defined as the difference of thermal anomalies between the running north and south regions (bounded by 22°N) within a certain longitude range. The light- and dark-blue values denote correlation coefficients above the 10% and 5% significance levels, respectively. The yellow value represents the YunGuiP-BeibuG thermal contrast studied in the paper

SCSSMOD at the interannual timescale, Fig. 7a displays the PDF distribution of SCSSMOD with respect to the positive (red) or negative (blue) thermal contrast index. These two PDFs are significantly separated at the 5% confidence level based on the nonparametric Kolmogorov–Smirnov two-sample test (Simard and L'Ecuyer 2011), and during years of positive thermal contrast, the SCSSM tends to onset earlier with the median date left of the average onset date during 1979–2019. During years of negative thermal contrast, however, the SCSSM tends to occur later. In addition, for an early (a delayed) SCSSMOD, the probability is obviously higher under the condition of positive (negative) thermal contrast, as suggested by the larger value of red (blue) PDF (Fig. 7a). The scatter plot of the thermal contrast index versus the SCSSMOD during 1979–2019 confirms this information (Fig. 7b). Approximately 68.2% of early monsoon onset years (15 out of 22) occurred during years with a positive thermal contrast, while about 78.9% of delayed onset years (15 out of 19) emerged during years with a negative thermal contrast (Fig. 7b). These results validate that the spring YunGuiP-BeibuG land-sea thermal contrast can be an effective seasonal predictor for SCSSMOD at the interannual timescale.

4.2 ECHAM6.3 numerical simulation

The above results are obtained by the correlation/regression analysis, but it is difficult to tell from the causality. Hence, to confirm above physical processes, the ECHAM6.3 is further applied in the study. In ECHAM6.3, two sensitivity experiments named the Posi-exp and Nega-exp were conducted. They were forced by the observed March–April Q1 anomalies at levels over the YunGuiP and BeibuG regions, which were regressed onto the normalized raw and reversed thermal contrast index during 1979–2019, respectively. As such, the Posi-exp represents the atmospheric thermal condition of heat source in YunGuiP and heat sink in BeibuG to enhance the climatological land-sea thermal contrast in spring (Fig. 8a), while the Nega-exp represents the opposite condition to weaken the climatological land-sea thermal contrast (Fig. 8b). These added Q1 anomalies in the two targeted areas are superimposed onto the modelled air temperature from March 1 to April 30. In order to better highlight the atmospheric responses to YunGuiP-BeibuG thermal contrast in simulation, the regressed Q1 anomalies in the observation are doubled beforehand.

The composite differences between the Posi-exp and Nega-exp are presented (Fig. 8c–f). Results present that the land-sea thermal gradient is enlarged when YunGuiP warms and BeibuG cools in spring (Fig. 8a), forming an anomalous anticyclonic circulation over the WNP in the lower troposphere (Fig. 8c). South of the anticyclone, strong easterly anomalies are observed over the Maritime Continent. These easterly winds cause the low-level convergence ($\partial u/\partial x < 0$) and divergence ($\partial u/\partial x > 0$) to occur southwest and southeast of the Philippines, respectively, due to the interaction of circulation and terrain (Fig. 8d). As a result, the strongly above-than-normal and below-than-normal precipitation anomalies are excited in response to the low-level divergence field in spring (Fig. 8e). The above-than-normal precipitation anomalies in spring are primarily found over the southern SCS and then move northward in May towards the northern SCS (Fig. 8f). The latter in turn arises the low-level Rossby cyclonic circulation via the Matsuno-Gill mechanism (Gill 1980), motivating the eastward retreat of western Pacific subtropical high and significant westerly anomalies over the SCS (Fig. 8f) and causing an early SCSSMOD in May. The results obtain from the ECHAM6.3 numerical simulation are largely similar to those in observation and show comparable magnitudes, thus confirming the behind physical mechanisms. Nevertheless, these still exist some differences between simulation and observation. For example, the model simulated low-level wind response in the defined thermal regions especially in YunGuiP is different and even opposite (Fig. 8c) to that in observation (Fig. 5b). This can be understood by following aspects: Since we only add the YunGuiP heat source and BeibuG heat sink in ECHAM6.3, and as long as a positive (negative) heat forcing in model, a cyclonic (an anticyclonic) curve should emerge nearby. Consequently, the heat forcing in YunGuiP could induce the regional cyclonic anomaly (a small-scale cyclonic vorticity) in situ and the resultant low-level northerly winds there in ECHAM6.3. In the observation, however, there are other regions with significant heat anomalies (Fig. 5a), which are actually eliminated in model, and the changes in low-level winds may also be related to these heat anomalies.

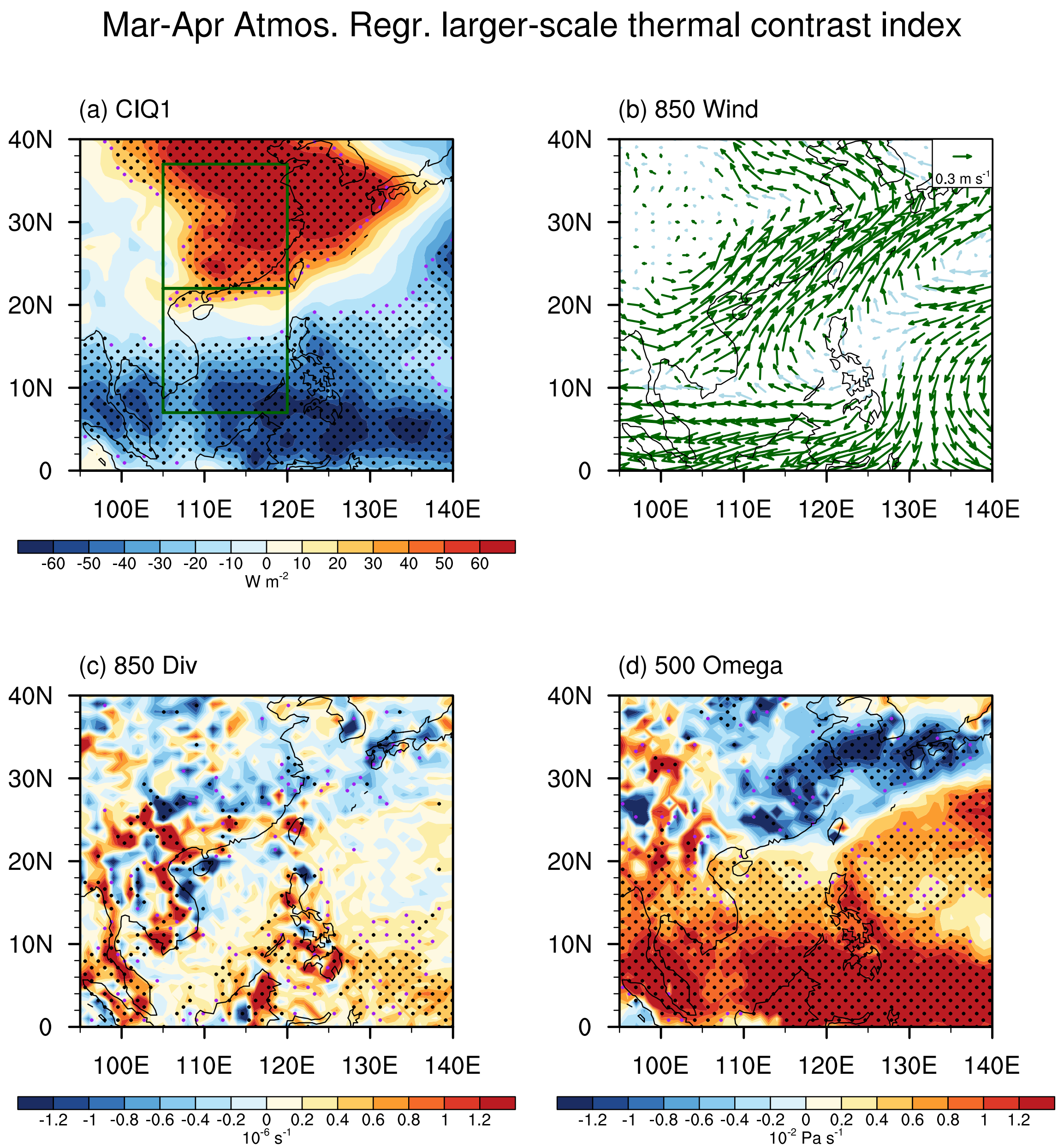

Fig. 9 Regression of the March–April **a** CIQ1 (shading, SI = 10 W m^{-2}), **b** 850 hPa winds (vector, unit: 0.3 m s^{-1}), **c** 850 hPa divergence (shading, SI = 0.2×10^{-6} s^{-1}), and **d** 500 hPa vertical velocity (shading, SI = 0.2×10^{-2} Pa s^{-1}) onto the normalized larger-scale thermal contrast index during 1979–2019, respectively. The purple and black dots indicate values statistically significant at the 10% and 5% significance levels, respectively. The green rectangles in (**a**) indicate the regions between South China (22°–37°N, 105°E–120°E) and the whole of SCS (7°–22°N, 105°E–120°E) to define the larger-scale thermal contrast index, respectively. The green and light-blue vectors in (**b**) represent values above and below the 10% significance levels, respectively

Therefore, the regional low-level wind responses are theoretically different between simulation and observation.

5 Discussion

From Figs. 2a and 5a, it can be seen that the maximum range of CIQ1 is not limited to YunGuiP, but seems to extend more northward and eastward in South China. The thermal anomaly in YunGuiP is just a small part of anomalies in a much larger region. Although the triggering effects of spring YunGuiP-BeibuG land-sea thermal

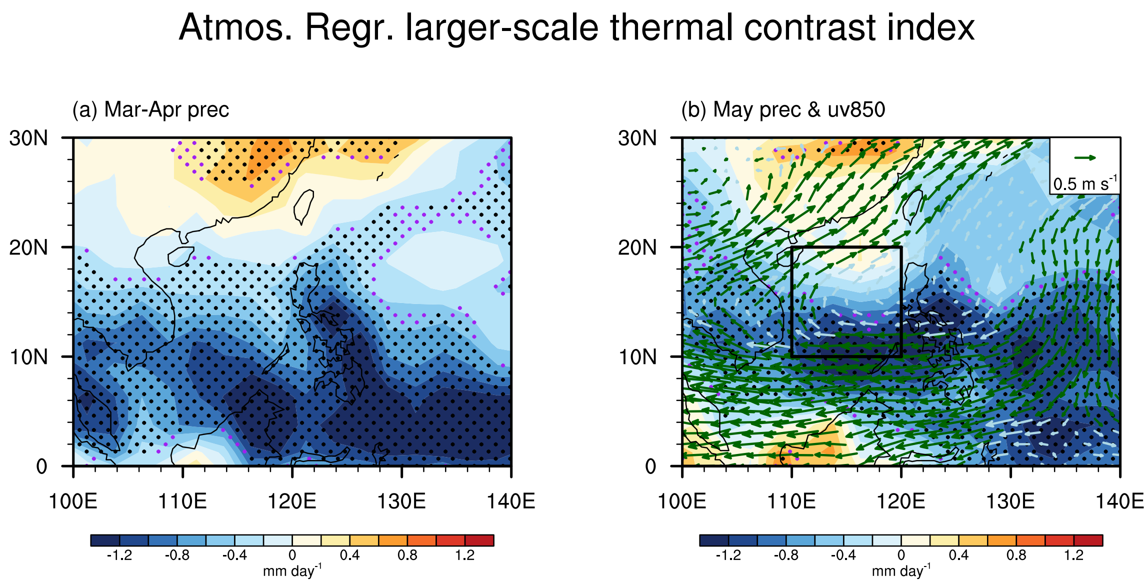

Fig. 10 Same as Fig. 9, but for regression of the **a** March–April precipitation (shading, SI = 0.2 mm day^{-1}) and **b** May precipitation (shading, SI = 0.2 mm day^{-1}) superimposed by the 850 hPa winds (vector, unit: 0.5 m s^{-1}) anomalies onto the normalized larger-scale thermal contrast index during 1979–2019, respectively. The black rectangle in (**b**) indicates the SCS region (10°–20°N, 110°E–120°E)

contrast on the variations of SCSSMOD at the interannual timescale are apparent through observation analysis and numerical simulation, one may also wonder why this study chooses such small thermal regions instead of larger-scale ones to explore the influence on monsoon establishment. We have to acknowledge that the maximum heating centre is not strictly within the defined scope of YunGuiP, but the thermal contrast between YunGuiP and BeibuG is actually the most significant heating precursor related to the SCSSMOD variations at the interannual timescale. To validate this point, we calculate the correlation coefficients between different land-sea thermal contrast indices defined from small to large regions and the SCSSMOD during 1979–2019 (Table 1). Result shows that a larger land-sea thermal contrast region, a smaller and more insignificant relationship with the SCSSMOD. Among them, the thermal contrast between the Yun-Gui Plateau and Beibu Gulf is the most significant one.

To illustrate the reason why the relationship between larger-scale land-sea thermal contrast regions and the SCSSMOD has weakened, here we take the larger-scale thermal regions between South China (22°–37°N, 105°E–120°E) and the whole of SCS (7°–22°N, 105°E–120°E) as an example. Actually, when selecting larger-scale regions to define the thermal contrast index in spring, the land-sea heating difference is stronger with larger spatial-scale (Fig. 9a). It can result in a stronger anticyclonic anomaly over the WNP (Fig. 9b), in which the easterly/northeasterly winds on the south side are stronger and cause larger low-level divergence effects (Fig. 9c). The low-level divergence over the tropical western Pacific is caused by $\partial v/\partial y > 0$ (east of 126°E) and $\partial u/\partial x > 0$ (west of 126°E) (Fig. 9b), resulting in enhanced downward motions in the mid-level there (Fig. 9d). Then, below-than-normal precipitation are subsequently excited over the tropical western Pacific in spring (Fig. 10a). The decreased precipitation anomalies migrate northward towards the central SCS in May and trigger an anomalous anticyclone over the WNP via the Matsuno-Gill mechanism (Fig. 10b). As a result, SCS is located at the centre of the excited anticyclone, and the zonal wind anomalies in the southern and northern parts almost cancel out each other with the smaller value at −0.11 m s^{-1}, thus having insignificant impact on the variations of SCSSMOD ($r \sim 0.16$, Table 1). In contrast, when selecting smaller-scale regions to define the thermal contrast index in spring such as the Yun-Gui plateau and Beibu Gulf, the simulated anticyclone over the WNP is weaker with smaller spatial-scale in spring, and its position is more northward (Fig. 5b). Then, it results in the active convection in the tropical western Pacific via the friction convergence, which persists into May and excites an anomalous low-level cyclone over the SCS (Fig. 6), promoting an early SCSSMOD. The above results indicate that the impacts of different spatial-scale thermal contrast on regional climate change are different, and when study the

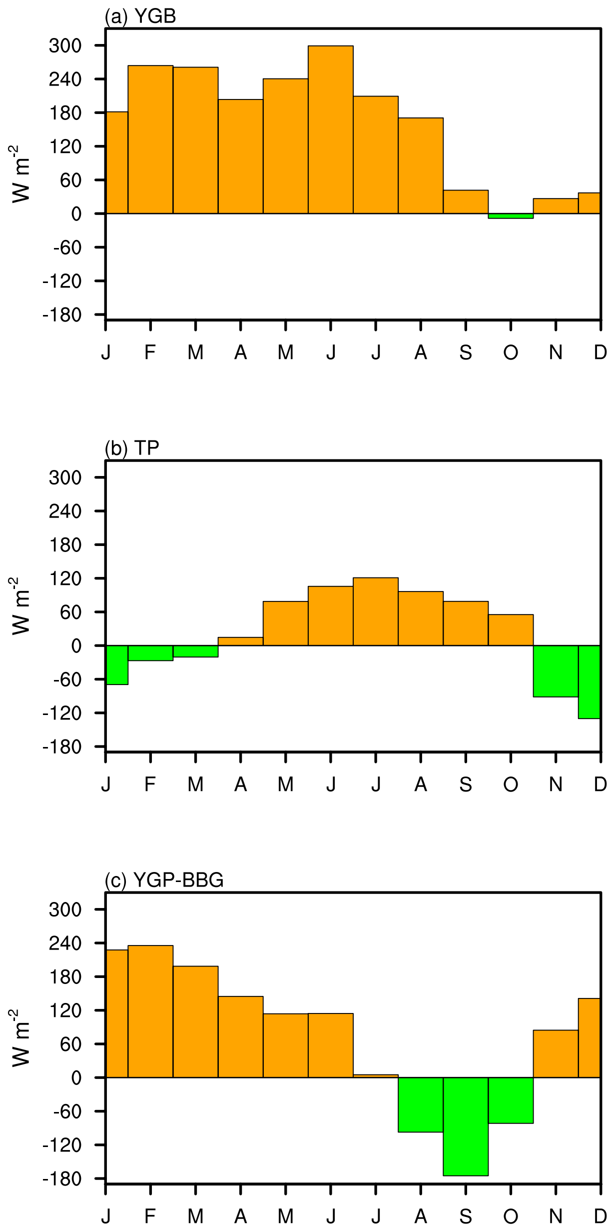

Fig. 11 Annual cycle of area-mean CIQ1 (unit: W m^{-2}) in **a** Yun-Gui plateau, **b** Tibet plateau, and **c** the thermal difference between Yun-Gui plateau and Beibu Gulf, respectively

variations of SCSSM onset, we may also need to focus on some small-scale signals.

Despite the region of YunGuiP is relatively small, it is a heat source with strong persistence from spring and summer (Fig. 11a). In spring, the diabatic heating in YunGuiP is even larger than that in Tibet plateau (Fig. 11b). Therefore, its thermal contrast with BeibuG can release a large number of diabatic heating in spring toward atmosphere (Fig. 11c), and then excite large-scale circulation anomalies (Fig. 5).

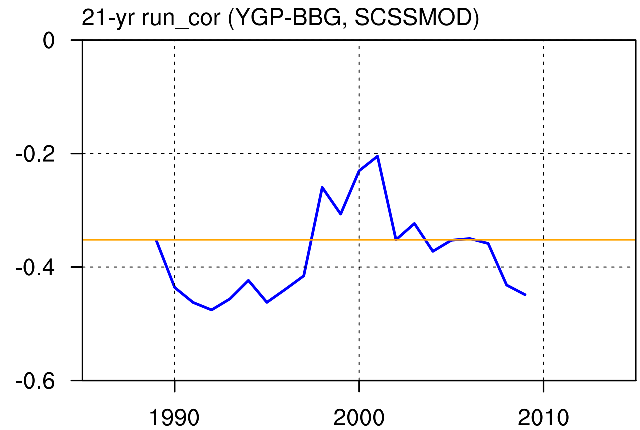

Fig. 12 The 21-year running correlation coefficients between the SCSSMOD and the YunGuiP-BeibuG thermal contrast index. The horizontal yellow line denotes the correlation being significant at the 10% significance level

On the other hand, the period from March to April coincides with the transition condition of atmospheric circulation over the SCS and WNP from winter to summer. At this time, the winter circulation is declining and the summer circulation has not yet been established. Once there is a large atmospheric heating meanwhile (Fig. 5a), it will quickly change the basic flow field, causing significant circulation anomalies and impact the SCSSMOD subsequently. Based on above considerations, the YunGuiP-BeibuG thermal contrast can be regarded as the key heating precursor for SCSSMOD at the interannual timescale.

Furthermore, although we have confirmed that the anticyclonic anomaly over the WNP and the convective activity over the tropical western Pacific in spring can be triggered by the YunGuiP-BeibuG thermal contrast through observation and model, we cannot rule out the possibility that these atmospheric circulation anomalies may in turn affect the regional thermal states. On the one hand, the tropical convection activity around Sumatra and the Indochina Peninsula can excite the low-level circulation anomalies over the WNP and affect the changes of WNP anticyclone (He et al. 2006). On the other hand, the anticyclonic anomaly could cause the thermal anomalies in YunGuiP via the southwesterly winds-induced low-level convergence and ascending motion, impacting the local land-sea thermal contrast. Exploring such a two-way interaction and their synergistic impact on the interannual variations of SCSSMOD has important scientific significance, and should be conducted in future work.

6 Conclusion

Through observation analysis and numerical simulation, this study reveals the triggering effects of spring thermal contrast between YunGuiP and BeibuG on the variations of SCSSMOD at the interannual timescale: The March–April land-sea thermal contrast associated with warm YunGuiP and cold BeibuG, superimposed on the background atmospheric thermal conditions, can lead to an anomalous anticyclone over the WNP. The easterly anomalies south of the anticyclone then cause the strengthening of precipitation and active convection over the tropical western Pacific via the friction convergence. The latter persists into May and move northward towards the SCS. As a result, an anomalous low-level cyclone is excited over the WNP via the Matsuno-Gill Rossby response, and further promotes the eastward retreat of western Pacific subtropical high. South of the cyclonic circulation, there are significant westerly wind anomalies over the SCS in May. These westerly anomalies accelerate the seasonal transition of zonal winds from easterly to westerly winds, causing an early SCSSMOD. The opposite happens when the thermal contrast reverses.

Although the YunGuiP-BeibuG spring thermal contrast can significantly impact the SCSSMOD at the interannual timescale, we still have no idea if their relationship is stable in recent decades. To address the issue, Fig. 12 displays the 21-yr running correlation between the defined thermal contrast index and the SCSSMOD, and it is found that their relationship is significant before the late-1990s but then experiences a brief weakening period until the early-2000s. Such relationship recovers afterwards, in which the ENSO-SCSSM relation start to weaken (Hu et al. 2022). Considering the weakened ENSO-SCSSM relation may cause a challenge to perform a skilful seasonal prediction for SCSSMOD and the effects of the studied thermal contrast in the paper on SCSSMOD are independent of ENSO, the spring YunGuiP-BeibuG thermal contrast can be an effective precursory factor to monitor and predict the variations of SCSSMOD during the challenging period.

Acknowledgements We would like to thank three anonymous reviewers for their comments that have improved our manuscript. The National Natural Science Foundation of China (42030603, 42205061, and 42022035) and the Natural Science Foundation of Yunnan Province (202302AN360006) funded this study.

Funding National Natural Science Foundation of China, 42030603, Jie Cao, 42205061, ZIZHEN DONG, 42022035, Ruowen Yang, Natural Science Foundation of Yunnan Province, 202302AN360006, Ruowen Yang.

Data availability The GPCP precipitation data were downloaded from (https://www.ncei.noaa.gov/data/global-precipitation-climatology-project-gpcp-monthly/access/). The OLR dataset was downloaded from (https://psl.noaa.gov/thredds/catalog/Datasets/interp_OLR/catalog.html). The ERA5 dataset was downloaded from (https://cds.climate.copernicus.eu/cdsapp#!/search?type=dataset).

Declarations

Conflict of interest The authors declare no conflict of interest.

References

Adler RF, George JH, Alfred C et al (2003) The Version-2 global precipitation climatology project (GPCP) monthly precipitation analysis (1979–Present). J Hydrometeorol 4:1147–1167. https://doi.org/10.1175/1525-7541(2003)004%3c1147:TVGPCP%3e2.0.CO;2

Chen H, Wang L (2023) Mechanism of the late summer monsoon onset in Bay of Bengal and South China Sea during 2021: Impacts of intraseasonal oscillation and local thermal contrast. Dyn Atmos Oceans 101:101348. https://doi.org/10.1016/j.dynatmoce.2022.101348

Chen J, Zuo T, Wang H (2012) Response of the South China Sea summer monsoon onset to air-sea heat fluxes over the Indian Ocean. Chin J Oceanol Limnol 30:974–979. https://doi.org/10.1007/s00343-012-1255-z

Chen W, Hu P, Huangfu J (2022) Multi-scale climate variations and mechanisms of the onset and withdrawal of the South China Sea summer monsoon. Sci China Earth Sci 65:1030–1046. https://doi.org/10.1007/s11430-021-9902-5

Choudhury D, Nath D, Chen W (2022) Key features associated with the early and late South China summer monsoon onset. Theoret Appl Climatol 147:99–108. https://doi.org/10.1007/s00704-021-03826-3

Chow KC, Liu Y, Chan JCL et al (2006) Effects of surface heating over Indochina and India landmasses on the summer monsoon over South China. Int J Climatol 26:1339–1359. https://doi.org/10.1002/joc.1310

Deng K, Yang S, Gu D et al (2020) Record-breaking heat wave in southern China and delayed onset of South China Sea summer monsoon driven by the Pacific subtropical high. Clim Dyn 54:3751–3764. https://doi.org/10.1007/s00382-020-05203-8

Ding Y, Chan JCL (2005) The East Asian summer monsoon: an overview. Meteorol Atmos Phys 89:117–142. https://doi.org/10.1007/s00703-005-0125-z

Ding Y, Liu Y, Song Y et al (2015) From MONEX to the global monsoon: a review of monsoon system research. Adv Atmos Sci 32:10–31. https://doi.org/10.1007/s00376-014-0008-7

Dong Z, Wang L, Xu P et al (2021) Interdecadal variation of the wintertime precipitation in Southeast Asia and its possible causes. J Clim 34:3503–3521. https://doi.org/10.1175/JCLI-D-20-0480.1

Dong Z, Wang L, Gong H et al (2022) A skilful seasonal prediction for wintertime rainfall in southern Thailand. Int J Climatol 42:10048–10061. https://doi.org/10.1002/joc.7882

Dong Z, Wang L, Gui S et al (2023) Diminished impact of the East Asian winter monsoon on the Maritime Continent rainfall after the late-1990s tied to weakened Siberian high–Aleutian low covariation. J Geophys Res: Atmos 128:e2022. https://doi.org/10.1029/2022JD037336

Feng J, Wang L, Chen W et al (2010) Different impacts of two types of Pacific Ocean warming on Southeast Asian rainfall during boreal winter. J Geophys Res 115:D24122. https://doi.org/10.1029/2010JD014761

Feng J, Wang F, Yu L et al (2021) Revisiting the relationship between Indo-Pacific heat content and South China Sea summer monsoon onset during 1980–2020. Int J Climatol 41:1998–2016. https://doi.org/10.1002/joc.6943

Gill AE (1980) Some simple solutions for heat-induced tropical circulation. Q J R Meteorol Soc 106:447–462. https://doi.org/10.1002/qj.49710644905

Giorgetta MA, Jungclaus J, Reick CH et al (2013) Climate and carbon cycle changes from 1850 to 2100 in MPI-ESM simulations for the Coupled Model Intercomparison Project phase 5 [Software]. J Adv Model Earth Syst 5:572–597. https://doi.org/10.1002/jame.20038

Gui S, Yang R, Cao J et al (2020) Precipitation over East Asia simulated by ECHAM6.3 with different schemes of cumulus convective parameterization. Clim Dyn 54:4233–4261. https://doi.org/10.1007/s00382-020-05226-1

Gui S, Su Q, Yang R et al (2022) Association of the shift of the South Asian high in June with the diabatic heating in spring. Clim Dyn 59:869–886. https://doi.org/10.1007/s00382-022-06161-z

He J, Zhu Z (2015) The relation of South China Sea monsoon onset with the subsequent rainfall over the subtropical East Asia. Int J Climatol 35:4547–4556. https://doi.org/10.1002/joc.4305

He J, Wen M, Wang L et al (2006) Characteristics of the onset of the Asian summer monsoon and the importance of Asian-Australian ″land bridge″. Adv Atmos Sci 23:951–963. https://doi.org/10.1007/s00376-006-0951-z

He B, Zhang Y, Li T et al (2017) Interannual variability in the onset of the South China Sea summer monsoon from 1997 to 2014. Atmos Ocean Sci Lett 10:73–81. https://doi.org/10.1080/16742834.2017.1237853

Hersbach H, Bell B, Berrisford P et al (2020) The ERA5 global reanalysis. Q J R Meteorol Soc 146:1999–2049. https://doi.org/10.1002/qj.3803

Hu P, Chen W (2018) The relationship between the East Asian winter monsoon anomaly and the subsequent summer monsoon onset over the South China Sea and the impact of ENSO. Clim Environ Res 23:401–412. https://doi.org/10.3878/j.issn.1006-9585.2017.17026. (**in Chinese**)

Hu P, Chen W, Chen S et al (2020) Extremely early summer monsoon onset in the South China Sea in 2019 following an El Niño Event. Mon Weather Rev 148:1877–1890. https://doi.org/10.1175/MWR-D-19-0317.1

Hu P, Chen W, Chen S et al (2022) The weakening relationship between ENSO and the South China Sea summer monsoon onset in recent decades. Adv Atmos Sci 39:443–455. https://doi.org/10.1007/s00376-021-1208-6

Huangfu J, Chen W, Wang X et al (2018) The role of synoptic-scale waves in the onset of the South China Sea summer monsoon. Atmos Science Letters 19:e858. https://doi.org/10.1002/asl.858

Hung R, Gu L, Zhou L et al (2006) Impact of the thermal state of the tropical western Pacific on onset date and process of the South China Sea summer monsoon. Adv Atmos Sci 23:909–924. https://doi.org/10.1007/s00376-006-0909-1

Jiang N, Zhu C (2021) Seasonal forecast of South China Sea summer monsoon onset disturbed by cold tongue La Niña in the past decade. Adv Atmos Sci 38:147–155. https://doi.org/10.1007/s00376-020-0090-y

Jiang X, Wang Z, Li Z (2018) Signature of the South China Sea summer monsoon onset on spring-to-summer transition of rainfall in the middle and lower reaches of the Yangtze River basin. Clim Dyn 51:3785–3796. https://doi.org/10.1007/s00382-018-4110-x

Kajikawa Y, Wang B (2012) Interdecadal change of the South China Sea summer monsoon onset. J Clim 25:3207–3218. https://doi.org/10.1175/JCLI-D-11-00207.1

Lau KM, Yang S (1997) Climatology and interannual variability of the southeast asian summer monsoon. Adv Atmos Sci 14:141–162. https://doi.org/10.1007/s00376-997-0016-y

Li Y, Yang S, Deng Y et al (2020) Signals of spring thermal contrast related to the interannual variations in the Onset of the South China Sea summer monsoon. J Clim 33:27–38. https://doi.org/10.1175/JCLI-D-19-0174.1

Liebmann B, Smith CA (1996) Description of a complete (interpolated) outgoing longwave radiation dataset. Bull Am Meteor Soc 77:1275–1277. https://doi.org/10.1175/1520-0477-77.6.1274

Liu B, Zhu C (2019) Extremely late onset of the 2018 South China Sea summer monsoon following a La Niña event: effects of triple SST anomaly mode in the North Atlantic and a Weaker Mongolian cyclone. Geophys Res Lett 46:2956–2963. https://doi.org/10.1029/2018GL081718

Liu X, Li Q, He J et al (2009) Effects of the thermal contrast between Indo-China Peninsula and South China Sea on SCS monsoon onset. Acta Meteorologica Sinica 67:100–107 (**in Chinese**)

Liu B, Liu Y, Wu G et al (2015) Asian summer monsoon onset barrier and its formation mechanism. Clim Dyn 45:711–726. https://doi.org/10.1007/s00382-014-2296-0

Liu B, Zhu C, Yuan Y et al (2016) Two types of interannual variability of South China Sea summer monsoon onset related to the SST anomalies before and after 1993/94. J Clim 29:6957–6971. https://doi.org/10.1175/JCLI-D-16-0065.1

Lu M-M, Sui C-H, Sun J et al (2020) Influences of subseasonal to interannual oscillations on the SCS summer monsoon onset in 2018. Terr Atmos Ocean Sci 31:197–209. https://doi.org/10.3319/TAO.2020.02.25.01

Luo M, Leung Y, Graf H-F et al (2016) Interannual variability of the onset of the South China Sea summer monsoon. Int J Climatol 36:550–562. https://doi.org/10.1002/joc.4364

Ma L, Jiang Z (2020) Improved leading modes of interannual variability of the Asian-Australian monsoon in an AGCM via incorporating a stochastic multicloud model. Clim Dyn 54:759–775. https://doi.org/10.1007/s00382-019-05025-3

Maloney ED, Hartmann DL (1998) Frictional moisture convergence in a composite life cycle of the Madden–Julian oscillation. J Clim 11:2387–2403. https://doi.org/10.1175/1520-0442(1998)011%3c2387:FMCIAC%3e2.0.CO;2

Martin GM, Chevuturi A, Comer RE et al (2019) Predictability of South China Sea summer monsoon onset. Adv Atmos Sci 36:253–260. https://doi.org/10.1007/s00376-018-8100-z

Shao X, Huang P, Huang R-H (2014) A review of the South China Sea summer monsoon onset. Adv Earth Sci 29:1126–1137 (**in Chinese**)

Shao X, Huang P, Huang R-H (2015) Role of the phase transition of intraseasonal oscillation on the South China Sea summer monsoon onset. Clim Dyn 45:125–137. https://doi.org/10.1007/s00382-014-2264-8

Simard R, L'Ecuyer P (2011) Computing the two-sided Kolmogorov-smirnov distribution. J Stat Softw 39:1–18. https://doi.org/10.18637/jss.v039.i11

Wang B, LinHo, Zhang Y et al (2004) Definition of South China Sea monsoon onset and commencement of the East Asia Summer Monsoon. J Clim 17:699–710. https://doi.org/10.1175/2932.1

Wang B, Huang F, Wu Z et al (2009) Multi-scale climate variability of the South China Sea monsoon: A review. Dyn Atmos Ocean 47:15–37. https://doi.org/10.1016/j.dynatmoce.2008.09.004

Wang L, Dai A, Guo S et al (2017) Establishment of the South Asian high over the Indo-China Peninsula during late spring to summer. Adv Atmos Sci 34:169–180. https://doi.org/10.1007/s00376-016-6061-7

WangLinHo B (2002) Rainy season of the Asian-Pacific summer monsoon. J Clim 15:386–398. https://doi.org/10.1175/1520-0442(2002)015%3c0386:RSOTAP%3e2.0.CO;2

Webster PJ, Yang S (1992) Monsoon and enso: selectively interactive systems. Q J R Meteorol Soc 118:877–926. https://doi.org/10.1002/qj.49711850705

Wen D, Gui S, Cao J (2024a) Impact of May atmospheric latent heating over the Southeast Asian low-latitude highlands on interannual variability in the Meiyu onset date. Atmos Res 298:107158. https://doi.org/10.1016/j.atmosres.2023.107158

Wen D, Yang Y, Cao J (2024b) Interannual covariation of the thermal conditions of the southeast asian low-latitude highlands and summer East Asia-Pacific teleconnection pattern. Clim Dyn 62:759–771. https://doi.org/10.1007/s00382-023-06943-z

Wu G, Liu Y, He B et al (2012) Thermal controls on the Asian summer monsoon. Sci Rep 2:404. https://doi.org/10.1038/srep00404

Xie A, Chung Y-S, Liu X et al (1998) The interannual variations of the summer monsoon onset over the South China Sea. Theoret Appl Climatol 59:201–213. https://doi.org/10.1007/s007040050024

Xu L, Li Z-L (2021) Impacts of the wave train along the Asian Jet on the South China Sea summer monsoon onset. Atmosphere 12:1227. https://doi.org/10.3390/atmos12091227

Xu Q, Chen W, Song L (2022) Two leading modes in the evolution of major sudden stratospheric warmings and their distinctive surface influence. Geophys Res Lett 49:e2021GL09543. https://doi.org/10.1029/2021GL095431

Yanai M, Li C, Song Z (1992) Seasonal heating of the Tibetan Plateau and its effects on the evolution of the Asian summer monsoon. J Meteorol Soc Jpn 79:419–434. https://doi.org/10.2151/jmsj1965.70.1B_319

Yang Y, Yang Y, Cao J (2023) Seasonal variability of diabatic heating in the Southeast Asian low-latitude highlands. Theoret Appl Climatol 152:1311–1323. https://doi.org/10.1007/s00704-023-04460-x

Yang Y, Wen D, Gui S et al (2024) Thermal and mechanical effects of the Southeast Asian low-latitude highlands on the East Asian summer monsoon. J Clim 37:349–361. https://doi.org/10.1175/JCLI-D-22-0814.1

Yuan Y, Zhou W, Chan JCL et al (2008) Impacts of the basin-wide Indian Ocean SSTA on the South China Sea summer monsoon onset. Int J Climatol 28:1579–1587. https://doi.org/10.1002/joc.1671

Zhou W, Chan JCL (2007) ENSO and the South China Sea summer monsoon onset. Int J Climatol 27:157–167. https://doi.org/10.1002/joc.1380

Zhu Z, Li T (2017) Empirical prediction of the onset dates of South China Sea summer monsoon. Clim Dyn 48:1633–1645. https://doi.org/10.1007/s00382-016-3164-x